JACS
JOURNAL OF THE AMERICAN CHEMICAL SOCIETY
Article
pubs.acs.org/JACS

Avenaciolides: Potential MurA-Targeted Inhibitors Against Peptidoglycan Biosynthesis in Methicillin-Resistant *Staphylococcus aureus* (MRSA)

Ching-Ming Chang,[†,‡,§] Jeffy Chern,[†,§,∥] Ming-Yi Chen,[⊥] Kai-Fa Huang,[†] Chein-Hung Chen,[#] Yu-Liang Yang,[▽] and Shih-Hsiung Wu*[,†,‡,∥]

[†]Institute of Biological Chemistry, [§]Chemical Biology and Molecular Biophysics Program, Taiwan International Graduate Program, [#]Genomics Research Center, and [▽]Agricultural Biotechnology Research Center, Academia Sinica, Taipei 115, Taiwan

[‡]Institute of Biochemical Sciences and [∥]Department of Chemistry, National Taiwan University, Taipei 10617, Taiwan

[⊥]General Education Center, National Taipei University of Nursing and Health Sciences, Taipei 112, Taiwan

Supporting Information

ABSTRACT: Discovery of new antibiotics for combating methicillin-resistant *Staphylococcus aureus* (MRSA) is of vital importance in the post-antibiotic era. Here, we report four avenaciolide derivatives (**1**−**4**) isolated from *Neosartorya fischeri*, three of which had significant antimicrobial activity against MRSA. The morphology of avenaciolide-treated cells was protoplast-like, which indicated that cell wall biosynthesis was interrupted. Comparing the structures and minimum inhibitory concentrations of **1**−**4**, the α,β-unsaturated carbonyl group seems to be an indispensable moiety for antimicrobial activity. Based on a structural similarity survey of other inhibitors with the same moiety, we revealed that MurA was the drug target. This conclusion was validated by ^{31}P NMR spectroscopy and MS/MS analysis. Although fosfomycin, which is the only clinically used MurA-targeted antibiotic, is ineffective for treating bacteria harboring the catalytically important Cys-to-Asp mutation, avenaciolides **1** and **2** inhibited not only wild-type but also fosfomycin-resistant MurA in an unprecedented way. Molecular simulation revealed that **2** competitively perturbs the formation of the tetrahedral intermediate in MurA. Our findings demonstrated that **2** is a potent inhibitor of MRSA and fosfomycin-resistant MurA, laying the foundation for the development of new scaffolds for MurA-targeted antibiotics.

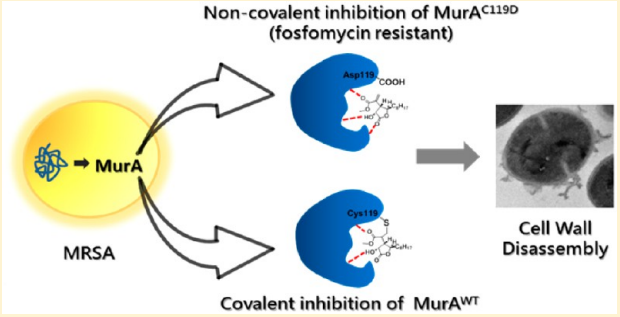

INTRODUCTION

The rapid rise in antimicrobial resistance is an emerging crisis for global public health.[1] Among Gram-positive drug-resistant bacteria, methicillin-resistant *Staphylococcus aureus* (MRSA) is the major pathogen responsible for nosocomial and community-acquired bacterial infections worldwide. MRSA can lead to a variety of human and animal diseases, including pneumonia, mastitis, osteomyelitis, endocarditis, skin infections, abscesses, food poisoning, toxic shock syndrome, and septicemia.[2−5] In the United States, the number of MRSA-related casualties has gradually exceeded those of HIV.[6]

Both Gram-positive and -negative bacteria are surrounded by a peptidoglycan (PG) cell wall (Figure 1) that protects the cell from destruction by osmotic pressure. Disrupting PG biosynthesis is an established approach for generating antimicrobial agents.[7] All enzymes involved in PG biosynthesis are essential for bacterial cell survival. The enzyme MurA (UDP-NAG enolpyruvyl transferase) catalyzes the first committed step in the cytoplasmic stage of PG biosynthesis (Figure 1). MurA catalyzes the transfer of enolpyruvate from phosphoenolpyruvate (PEP) to UDP-NAG (urinary *N*-acetyl-D-glucosaminidase, UNAG), releasing inorganic phosphate (Pi).[8] The deletion or inactivation of the *murA* gene is lethal in a variety of bacteria due to the loss of cell integrity and increased susceptibility to osmotic lysis.[9−11] Therefore, MurA is an attractive target for antibiotic discovery due to its essential role in microbial survival and its limited homology to mammalian proteins.

Fosfomycin resistance has recently gained considerable attention. Numerous reports indicate that fosfomycin-resistant bacteria, such as *Mycobacterium tuberculosis*, *Chlamydia thrachomatix*, and *Borrelia burgdorferi*,[12−15] protect themselves from fosfomycin through either mutations or by encoding counteracting proteins that inactivate or neutralize fosfomycin.[16−19] Fosfomycin, isolated from a natural product, is a clinical antibiotic used for the early treatment of pediatric gastrointestinal infections resulting from Shiga-like toxin-producing *Escherichia coli* (STEC)[17] as well as a first-line agent for treating bacterial urinary tract infections.[20] MurA has

Received: October 9, 2014
Published: December 18, 2014

DOI: 10.1021/ja510375f
J. Am. Chem. Soc. 2015, 137, 267−275

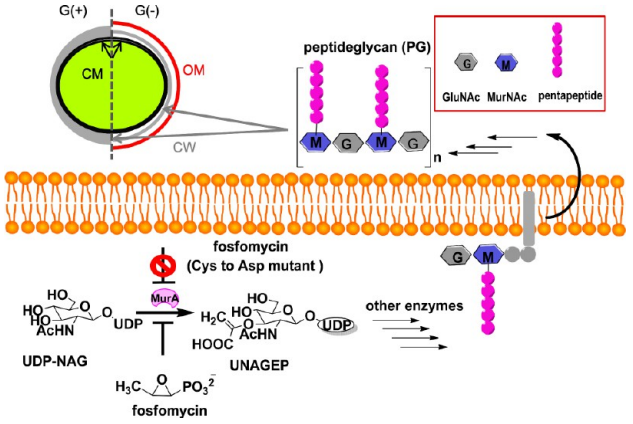

Figure 1. Schematic representation for the MurA reaction involved in the biosynthesis of PG (the main cell wall). The only MurA-targeted antibiotic, fosfomycin, is activated via cysteine. The top figure illustrates the different cell envelope components between Gram-positive and -negative bacteria. The cell envelope of G (+) bacteria comprises the cell wall (CW, gray line) and cell membrane (CM, black line). There is one more layer of outer membrane (OM, red line) outside the cell wall of G (−) bacteria.

been identified as the molecular target of fosfomycin.[21] Fosfomycin inhibits MurA activity by covalent alkylation of the highly conserved catalytic cysteine.[22−24] Because attack by the sulfhydryl group on the epoxide of fosfomycin is required for fosfomycin specificity and potency (Figure 1), the mutation of Cys-to-Asp confers natural fosfomycin resistance in certain organisms. Although other factors, such as *fosA* gene found in Gram-negative and *fosB* found in Gram-positive,[25−28] are responsible for fosfomycin resistance, only the Cys-to-Asp mutation on MurA results in totally fosfomycin resistance.

Natural products are excellent sources for drug discovery because of their potential as leads and scaffolds for the identification of unprecedented modes of action, pathways, and targets for the treatment of human diseases.[29,30] Therefore, we aimed to discover new lead compounds for combatting MRSA infections. In this study, we identified a methanol extract from indigenous *Neosartorya fischeri* in Hualien, Taiwan, with significant antimicrobial activity against MRSA. Using bioactivity-guided fractionation and isolation strategies, four avenaciolide derivatives (**1**−**4**; Figure 2) were purified, and their structures were determined. Using transmission electron

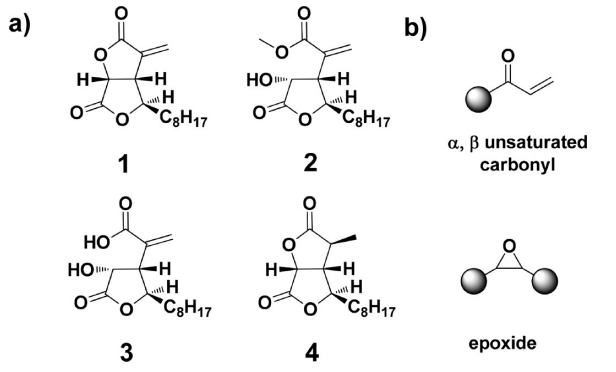

Figure 2. Avenaciolide derivatives isolated from *Neosartorya fischeri*. (a) Chemical structures of avenaciolides **1**−**4**. (b) Common electrophilic "warheads" used in targeted covalent inhibitors. Gray balls represent other pharmacophore structures.

microscopy (TEM) analyses, we demonstrated that the mechanism of the antimicrobial activities of **1**−**3** was the disruption of cell wall assembly. Using ^{31}P NMR spectroscopy, we identified MRSA MurA as the molecular target of **1**−**3**. Among the isolated compounds, **1** and **2** exhibited unexpected efficacy against MRSA MurA^{WT} and MurA^{C119D} (a fosfomycin-resistant mutant). Based on these results and the results of LC-MS/MS and docking calculations, we propose a mechanism for MRSA MurA inhibition. Thus, the identification of **2** as a MurA inhibitor provides insights into combating fosfomycin-resistant (Cys-to-Asp mutants) infections.

RESULTS AND DISCUSSION

The α,β-Unsaturated Carbonyl Moiety in Avenaciolides Is Essential for Disrupting Cell Wall Assembly. In this study, **1**−**4** (Figure 2a) were isolated from *N. fischeri*. The physicochemical properties of compounds **1**−**4** are summarized in the Supporting Information (Tables S2−4 and Figures S1−4). Among the isolated compounds, compounds **3** and **4** were new natural products.

1−**3** had greater antimicrobial activities against various Gram-positive bacteria, including *S. aureus* and *B. subtilis*, than against Gram-negative bacteria *E. coli* and *A. baumannii* (Table 1). The minimum inhibitory concentrations (MICs) of compounds **1** and **2** (16−32 μg mL^{-1}) indicated increased efficacy compared with **3** (256 μg mL^{-1}). TEM analysis indicated that the cells underwent profound changes in cell morphology and integrity in response to drug treatment. The TEM results also indicated that **1**−**3** induced cell wall disassembly (Figure 3). For example, the micrographs clearly demonstrated that the cell wall synthesis of MRSA (Figure 3b,c), *A. baumannii* (Figure 3h,i), *E. coli* (Figure S6g,h), and *B. subtilis* (Figure S6 b,c) were severely inhibited by **1** and **2**. TEM analysis also indicated that **3** was less potent than **1** and **2** against MRSA (Figure 3d) and *B. subtilis* (Figure S6d) and had no effect on *A. baumannii* (Figure 3j) and *E. coli* (Figure S6i). Consistent with the MIC results, no significant morphological changes were observed after treatment with **4** (Figure 3e,k; Figure S6e,i). Fosfomycin-treated cells appear as protoplasts, an indicator of cell wall disruption.[31] Therefore, we used fosfomycin (64 μg mL^{-1}) as a positive control (Figure 3f,l) to confirm that treatment with **1**−**3** inhibited cell wall assembly. Cell wall breakage and increasing coarseness of the cell surface were clearly visible in the TEM images of drug-treated cells compared with the untreated control cells (Figure 3a,g; Figure S6,f).

Based on the above results, we hypothesized that the antimicrobial activities of **1**−**3** were primarily mediated by interrupting cell wall assembly. Notably, the presence of the α,β-unsaturated carbonyl moiety, which is absent in **4**, appeared to be indispensable for antimicrobial activity as well as cell wall disassembly. The morphologies of the avenaciolide-treated cells and fosfomycin-treated cells were similar. Fosfomycin inhibits a key enzyme in PG synthesis.[21] Therefore, these observations suggested that the antibacterial activity of compounds **1**−**3** is due to the interruption of one of steps of bacterial cell wall biosynthesis, which ultimately leads to cell death.

Identification of MRSA MurA As a Molecular Target of Avenaciolides by ^{31}P NMR. To identify the enzyme in cell wall biosynthetic pathway that is targeted by avenaciolides, we initially examined avenaciolide or related analogues with a similar structural moiety and whose molecular target is reported to be involved in cell wall assembly.

DOI: 10.1021/ja510375f
J. Am. Chem. Soc. 2015, 137, 267−275

Table 1. Antimicrobial Activity and MurA IC_{50} of Avenaciolides 1−3

	1	2	3	Fos[a]
MIC (μg mL^{-1})				
S. aureus ATCC 29213	16	32	256	4
S. aureus ATCC 33592[c]	32	16	256	64
B. subtilis ATCC 23857	64	32	256	128
E. coli ATCC 25922	128	128	–[d]	64
A. baumannii 17978	256	256	–[d]	256
IC_{50} (μM)				
E. coli MurA	0.9 ± 1.11[b]	2.8 ± 1.22[b]	10.8 ± 1.13[b]	0.4 ± 1.16[b]
MRSA $MurA^{WT}$	8.3 ± 1.22[b]	6.7 ± 1.17[b]	71 ± 1.17[b]	1.6 ± 1.12[b]
MRSA $MurA^{C119D}$	21.5 ± 1.33[b]	7.9 ± 1.24[b]	–[d]	–[d]

[a]Fosfomycin was used as a reference standard in these two assays. [b]The standard deviation of the IC_{50} value was calculated based on five replicates. [c]Methicillin-resistant *S. aureus* strain [d]No activity

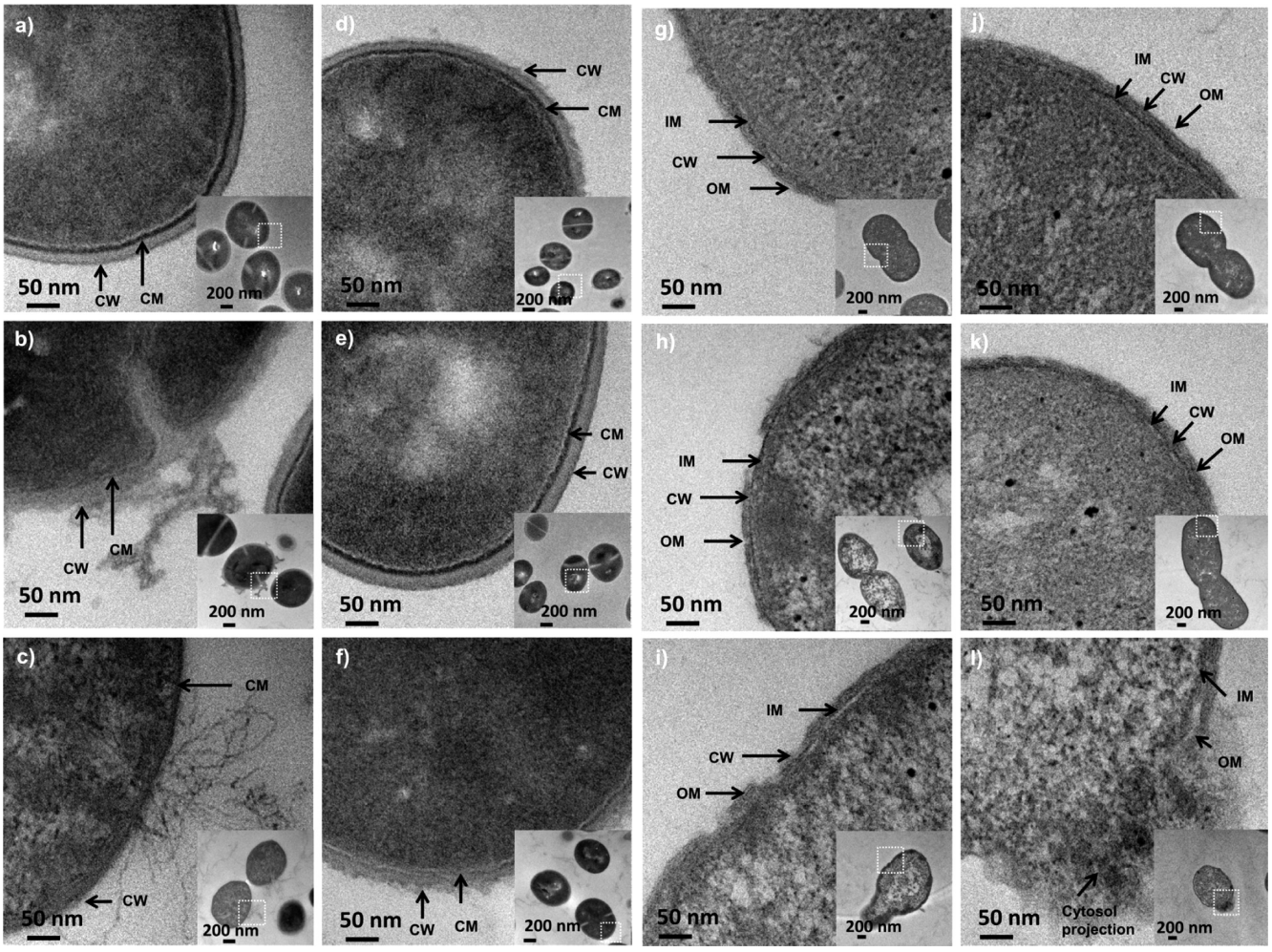

Figure 3. TEM of MRSA (a−f) and *A. baumannii* (g−l). (a and g) TEM micrographs of untreated *S. aureus* and *A. baumannii*. The healthy cells are round and intact. *S. aureus* had well-defined cell walls (CW) and cell membranes (CM); *A. baumannii* had smooth and continuous inner membranes (IM), CW, and outer membranes (OM). After incubation with 128 μg mL^{-1} **1** (b and h) and **2** (c and i) for 1 h, cell wall breakage and variability in wall thickness were observed. (d) Mild cell wall breakage was also observed after treatment with 128 μg mL^{-1} **3** for 1 h in *S. aureus*; this effect was not observed in *A. baumannii* (j). (e and k) **4** had no effect on cell morphology. (f and l) Fosfomycin (64 μg mL^{-1})-treated cells were used as a positive control.

Many molecules that contain the α,β-unsaturated carbonyl moiety,[26,27] which is also present in **1**−**3**, inhibit MurA. For example, sesquiterpene lactones (cnicin and cynaropicrin)[32] and some acrylic acid derivatives (tulipalines and tuliposides)[33] are natural products whose α,β-unsaturated carbonyl moiety is regarded as the essential scaffold similar to the substrate "PEP" for MurA inhibition. Therefore, we used MurA as the initial candidate for drug target validation.

A ^{31}P NMR spectroscopy-based method was used to efficiently confirm the targeting of MurA by **1**−**3**. By monitoring the release of Pi catalyzed by MRSA MurA, which is time-dependent (Figure S7), we determined that **1**−**3**

DOI: 10.1021/ja510375f
J. Am. Chem. Soc. 2015, 137, 267−275

inhibit MRSA MurA (Figure 4b, V−III). This result was confirmed by the lack of Pi signals after the addition of

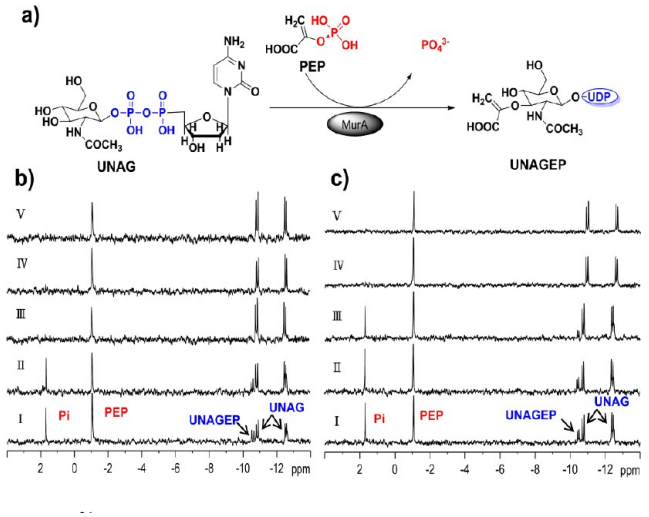

Figure 4. ^{31}P NMR spectroscopy screening of the inhibitory activities of 1−4 against MRSA MurA^{WT} and MRSA MurA^{C119D}. (a) MurA catalyzes the transfer of enolpyruvate from PEP to UNAG, releasing Pi. Both substrates (PEP, UNAG) and products (UNAGEP, Pi) were readily observed using ^{31}P NMR. (b) Addition of (V) **1**, (IV) **2**, and (III) **3** (1 mM) to the reaction solution (3.68 μM MRSA MurA^{WT}, 600 μM UNAG, and 800 μM PEP) inhibited Pi release. As expected, (II) **4** did not inhibit the MRSA MurA^{WT} reaction which showed the same results as (I) the control without any inhibitors. (c) Addition of (V) **1**, and (IV) **2** (1 mM) to the reaction solution (5 μM MRSA MurA^{C119D}, 600 μM UNAG, and 800 μM PEP) inhibited Pi release. However, (III) **3** and (II) fosfomycin (1 mM) did not interrupt the MRSA MurA^{C119D} reaction compared to (I) the control without any inhibitors.

inhibitors to the assay solution. No difference was observed between the reaction containing **4** (Figure 4, II) and the control (Figure 4, I), consistent with the MIC and TEM results.

In this study, we aimed to develop an efficient method for screening potential MurA inhibitors. Because both the substrates (UNAG and PEP) and products (UNAGEP and Pi) of MurA are all phosphonate compounds (Figure 4a), their signals can be measured using ^{31}P NMR spectroscopy. This approach offers an alternative for MurA-targeted inhibitor validation.

Avenaciolide 2 Has Unprecedented Potency against Fosfomycin-Resistant MurA. The Cys-to-Asp MurA variant is one of the most notorious mechanisms of fosfomycin resistance in bacteria.[12−14] Using a ^{31}P NMR spectroscopy-based method, we determined that MRSA MurA^{C119D} was resistant to fosfomycin (Figure 4c, II). Surprisingly, we found that **1** and **2** had inhibitory activity against MRSA MurA^{C119D} (Figure 4c, V and IV). In this study, both MRSA MurA^{WT} and MurA^{C119D} were used to quantify the IC$_{50}$ of **1**−**3** and fosfomycin using the malachite green assay[34] (Table 1). The IC$_{50}$s for **1**−**3** against MRSA MurA^{WT} were 6.7−71.0 μM, and the IC$_{50}$s for **1**−**2** against MRSA MurA^{C119D} were 21 and 7.9 μM, respectively.

To further understand whether this strong inhibition of **2** can also be observed *in vivo*, we thereby constructed and transformed an overexpression vector containing MurA^{C115D} to *E. coli* BL21 (DE3) (corresponding to the MurA^{C119D} in MRSA) to mimic a fosfomycin-resistant strain. By disk diffusion assay, we confirmed *E. coli* harboring pET28a::*murA*^{C115D} are strongly resistant to fosfomycin (MIC ≫128 μg)[24,35] comparing to those susceptible to fosfomycin (vector only control), but are inhibited significantly by **2** (MIC ∼ 2 μg) (Figure S8).

The IC$_{50}$s of all compounds (**1**−**3** and fosfomycin) were more potent against *E. coli* MurA than MRSA MurA, in contrast to the MICs results, which indicated greater potency against Gram-positive bacteria than Gram-negative bacteria (Table 1). One possible reason for this discrepancy is that less efficient drug influx into Gram-negative bacteria due to the outer membrane barrier (Figure 1) in contrast to fosfomycin efficiently delivered by two specific transporters.[36,37]

Many *S. aureus*[26] (34%) and *B. subtilis*[28] are less susceptible to fosfomycin due to the expression of FosB and results in transferring bacillithiol (BSH) onto the fosfomycin to counteract its potency. By PCR amplification and DNA sequencing, we confirmed that *S. aureus* ATCC33592 (MRSA) used in this study also contains *fosB* gene which is consistent with different MICs values for fosfomycin between *S. aureus* ATCC29213(4 μg mL^{-1}) and *S. aureus* ATCC33592(MRSA) (64 μg mL^{-1}) (Table 1). However, **2** still reveals potency toward *S. aureus* ATCC33592 (MRSA) (16 μg mL^{-1}) with even better efficacy than the that of fosfomycin (64 μg mL^{-1}). Overall, **2** was a potent inhibitor of MRSA MurA^{WT} as well as MurA^{C119D} and may provide an alternative treatment for fosfomycin-resistant infections.

Avenaciolides 1−3 Are Targeted Covalent Inhibitors (TCIs) of MRSA MurA. Fosfomycin inhibits *E. coli* MurA irreversibly by covalently binding to the Cys115 residue.[22−24] In small-molecule studies, we confirmed by mass spectrometry analysis that **1**−**3** reacted with L-cysteine and glutathione via Michael addition (Scheme S1 and Figures S10−13). Therefore, we hypothesized that **1**−**3** would act similarly in the MRSA MurA^{WT} active residue (Cys119) (Figure 5a). After incubating **1**−**3** with MRSA MurA^{WT}, three peptides were observed with monoisotopic masses consistent (within 5 ppm error) with Cys119 modified by Δmass +266 Da (+$C_{15}H_{22}O_4$), 298 Da (+$C_{16}H_{26}O_5$), and 284 Da (+$C_{15}H_{24}O_5$) (Figures 5b,c and S14). This observation of avenaciolide-derived adducts of MRSA MurA^{WT} Cys119 provides convincing evidence of protein S-acylation via Michael addition to the α,β-unsaturated carbonyl moiety in **1**−**3**. Consequently, these covalent inhibitors (**1**−**3**) represent TCIs that selectively covalently modify an essential catalytic residue in MRSA MurA^{WT}, leading to irreversible inhibition. However, the expected mass evidence for the reaction of L-aspartate with **1**−**3** via Michael addition was not observed, which suggests that the formation of covalent adducts is not the only prerequisite for the inhibitory efficacy of MRSA MurA^{C119D}. Thus, other noncovalent interactions should be involved to achieve selectivity for the MurA variant.

Recently, covalent drugs have been approved as treatments in diverse clinical applications and have made a major impact on human health.[38] Among covalent inhibitors, Michael addition, which targets the highly nucleophilic thiol group of cysteine residues,[39] is the most widely utilized reaction for achieving irreversible binding.[40] According to the literature and to our study, **1**−**3** and fosfomycin, which are defined as electrophilic "warheads" (Figure 2b), have the ability to target differentially modified cysteine residues to achieve drug selectivity.[41] The selectivity of a target-specific covalent inhibitor is described reasonably well by the following general equation (eq 1).

DOI: 10.1021/ja510375f
J. Am. Chem. Soc. 2015, 137, 267−275

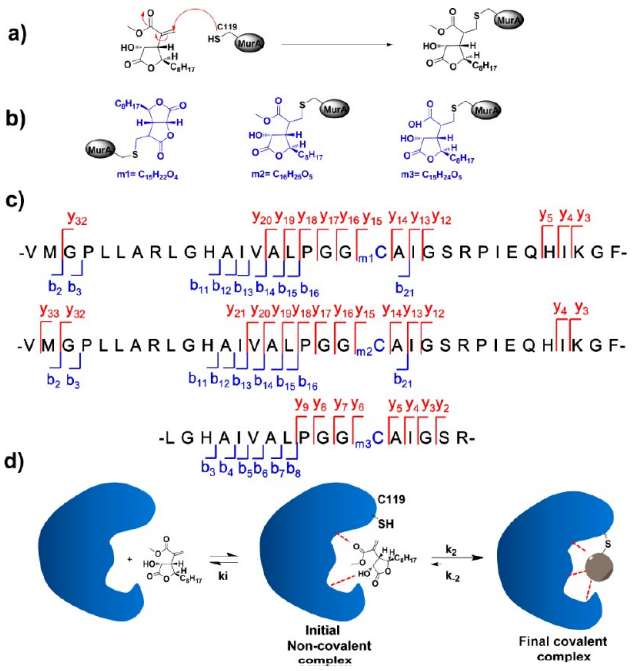

Figure 5. Mass spectrometry analysis of the avenaciolide-derived covalent modification of MRSA MurA. (a) The proposed Michael addition mechanism of **2** (a representative avenaciolide) for the observed S-alkylation of C119 in MRSA MurA^{WT}. (b) The expected structures and chemical formulas of **1**−**3** after attack on their α,β-unsaturated carbonyl moieties by the sulfhydryl group. (c) The avenaciolide-derived modifications by **1**−**3** were isolated to a single site, Cys119 (as indicated by Δmass +266 (m1), +298 (m2), +284 (m3) Da (see also Figure S14)). (d) The proposed mechanism of a target-specific covalent inhibitor (represented by **2**).

$$E + I \underset{K_i}{\rightleftharpoons} E \cdot I \overset{k_2}{\underset{k_{-2}}{\rightleftharpoons}} E\text{-}I \qquad (1)$$

Initial Non-covalent complex — Final covalent complex

First, the compound must bind noncovalently to the target protein, orienting its reactive electrophile near a specific nucleophile on the protein. Then, the final covalent complex is formed by the formation of a specific covalent bond between the compound and target protein. Therefore, TCIs have two orthogonal drivers for achieving selectivity toward their protein target: the initial binding step, K_i, and the subsequent chemical step, k_2 (eq 1).[42,43] Based on these theories, we proposed that **1**−**3** initially noncovalently bind to the target protein and, once the position of their α,β-unsaturated carbonyl moiety is appropriate, form a covalent bond, permanently disabling MurA (Figure 5d).

Fosfomycin, as a well-known TCI of MurA, should be first activated by Cys119 through nucleophilic attack on its epoxide. Therefore, the carboxylate group on Asp119 is not capable of forming a covalent bond with fosfomycin, providing a chemical rationale for the fosfomycin-resistant mechanism. Although covalent bonding to Cys119 serves as one intermediate during the catalytic turnover, the major route for this reaction relies on either Cys119 or Asp119 acting as the general acid for the protonation of C-3 on PEP (Figure S15).[44−47] The α,β-unsaturated carbonyl moiety of avenocilides as a PEP-mimicking molecule could be protonated by Asp119, suggesting another reason why **1**−**2** retain inhibitory activity against MRSA MurA^{C119D}.

Although other MurA inhibitors which have an α,β-unsaturated carbonyl moiety, such as cnicin[32] and acrylic acid derivatives of tulipalines and tuliposides,[33] were thought to react with the active site of *E. coli* MurA at cysteine via a Michael addition reaction, these hypotheses were not supported by mass spectrometry analysis. Our study provides the first evidence that the catalytic Cys119 forms a covalent adduct with α,β-unsaturated carbonyl moiety in MRSA MurA^{WT}.

Docking Calculations Revealed Possible Mechanisms for MRSA MurA Inhibition by Hindering of the Tetrahedral Intermediate (THI) Formation. To understand the possible molecular mechanisms underlying inhibition of MRSA MurA by **2**, homology modeling and docking calculations were used. Due to the lack of an available crystal structure, we initially constructed homology models of MRSA MurA^{WT} and MurA^{C119D} based on the structures from *S. pneumonia*,[48] *E. cloacae*,[49,50] *H. influenza*,[51] and *E. coli*[46,52] MurAs to minimize the differentials between the MurAs from Gram-positive and -negative bacterial strains. On the basis of the formation of a covalent MRSA MurA^{WT}-**2** complex (Figures 5b,c and S14), we docked **2** into the active site of MRSA MurA^{WT}, where **2** covalently binds to Cys119 (Figure 6a and the stereo figures are shown in Figure S16a). Our calculations suggested that the involvement of hydrogen bonds and hydrophobic interactions were the main factors responsible for stabilizing the docking complex (Figure 6a). Briefly, **2** forms three hydrogen bonds with the backbone of Cys119 and side chains of Arg124 and Arg374 in the MRSA MurA^{WT}-**2** complex (Figure 6a). Without the covalent constraint in MRSA MurA^{C119D}-**2** complex, **2** was docked onto MRSA MurA^{C119D} more flexibly, resulting in two additional hydrogen bonds to the side chain of Arg124 and Arg374 with relatively short distances. As a consequence, four hydrogen bonds in total were observed between MurA^{C119D} and **2**, which keeps **2** still binding well and retains its potency toward MRSA MurA^{C119D} (Figure 6a and the stereo figures are shown in Figure S16b). Moreover, the extended eight-carbon chain of **2** lies in a hydrophobic pocket surrounded by the residues Lys22, Lys93, Arg95, Met94, Leu373, and Arg400 in both MRSA MurA^{WT} and MurA^{C119D} (Figure 6b). These structural findings strongly support that **2** noncovalently binds to MurA first (MurA^{C119D}-**2** complex), and then the covalent adduct forms (MurA^{WT}-**2** complex) once the dynamic orientation is suitable for Michael addition.

Based on the binding mode of **2**, **1** may only form two hydrogen bonds with MRSA MurA due to the lack of the hydroxyl group (Figure 2). In addition, the rigid ring of the α,β-unsaturated lactone of **1** may also attenuate its hydrogen bonding to Arg374 (Figure 6a). Unlike **1** and **2**, the negatively charged carboxylic group in **3** may cause a strong electronic repulsion force when bound to MRSA MurA, due to its proximity to Asp308 (Figure 6a). This repulsion force may greatly alter the binding orientation of **3** and consequently result in the loss of hydrogen bonds with Arg124 and Arg374. To further understand the correlation between **2** and the reaction intermediates of MurA, we superimposed MurA in complex with either the tetrahedral intermediate (THI) (pdb code 3SWD)[46] or inorganic phosphate (pdb code 1RYW)[53] on MRSA MurA^{WT}-2 complex (Figure 6c,d). During PEP transfer, UNAG first binds to the active site of MurA.[22,54] The resulting complex is then in the proper orientation such that the 3′-

DOI: 10.1021/ja510375f
J. Am. Chem. Soc. 2015, 137, 267−275

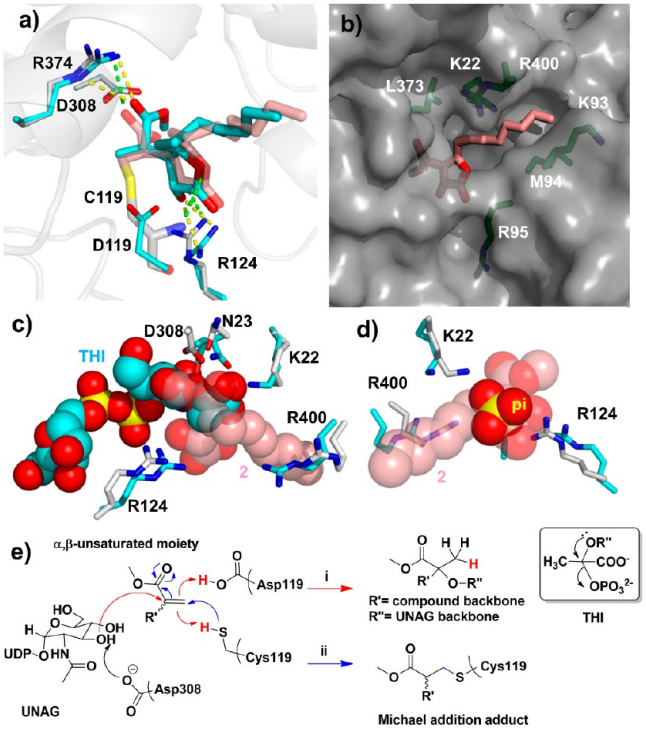

Figure 6. Modeled structures of MRSA MurA in complex with **2** and superimposition with the structures of MurA bound to the tetrahedral intermediate (THI) and the product Pi. (a) Superimposition of modeled structures of the MurA^{WT}-**2** (pink) and MurA^{C119D}-**2** (cyan) complexes. The hydrogen bonds are indicated with dotted lines and colored in green and yellow for MurA^{WT}-**2** and MurA^{C119D}-**2**, respectively. (b) Surface representation of the structure of MurA^{WT}-**2**. The compound extends into a hydrophobic pocket where the product Pi is released during catalysis. (c) Superimposition of MurA·THI (cyan, 3SWD) and MurA-**2** (pink in transparency). The MurA residues that interact with **2** or THI are shown as stick model. (d) Superimposition of MurA-Pi (yellow, 1RYW) and MurA^{WT}-**2** model (pink in transparency) structures. The aliphatic chain of **2** is located in the Pi binding site. (e) Mechanisms underlying MurA inhibition. (i) "dead-end" inhibition hypothesis (red arrows). Two is attacked by deprotonated UNAG, and the C═C of **2** is then accepting additional proton from either Asp119 or Cys119 forming an UNAG-**2** adduct which cannot be eliminated. (ii) MurA inhibition by catalytic Cys119 modification (blue arrows). Thiol gourp of catalytic Cys119 attacks the *α,β*-unsaturated moiety forming a Michael adduct.

hydroxyl group of UNAG attacks the C-2 of PEP, generating a THI with the participation of K22,[46,53] N23,[52,55] C119,[53,54,56] R124,[46,53] D308,[46,52] and R400[46,53] (in *S. aureus* numbering, Figures 6c and S9). MurA then catalyzes transformation of the THI to the final product, concomitant with phosphate trapping and release (K22, R124, and R400)[46,53] (Figure 6d). Our superimpositions suggested that **2** competitively inhibits the binding of the THI (Figure 6c) in addition to the trapping of phosphate (Figure 6d) by either steric interference or reacting with the key residues required for MurA activity which can also be found in MurA^{C119D}-**2** complex similarly.

To understand the roles played by *α,β*-unsaturated moiety in MurA inhibition, we proposed a "dead-end intermediate" hypothesis. During the catalytic process of MurA, the hydroxyl group on UNAG is first deprotonated and hence acts as a Lewis base attacking on the double bond of PEP, forming a tetrahedral intermediate (THI) via accepting an additional proton from Asp119 (Figure S15).[44] From our docking calculation, we observed the double bond of **2** is positioned in an optimal orientation not only for the hydroxyl group of UNAG to attack but also suitable for accepting the proton from Asp119 (Figure 6e, i). These findings makes UNAG-**2** adduct formation possible. Unlike the elimination of phosphate group after THI formation, the UNAG-**2** adduct without a good leaving group cannot be eliminated and thereby makes UNAG-**2** adduct a dead-end intermediate hindering the THI formation. Reconsidering the mechanism underlying MurA^{WT} inhibition, we believed both "dead-end" adduct (Figure 6e, i) and covalent modification on catalytic Cys119 (Figure 6e, ii) might occur. More works should be done to uncover the actual inhibition mechanism for this promising antifosfomycin-resistance agent.

Also, this hypothesis can be substantiated by MurA in complex with a natural product, cnicin, containing an *α,β*-unsaturated moiety.[57] In that co-crystal, an unusually UNAG-cnicin adduct forms first and then hinders the THI formation. Collectively, "dead-end" hypothesis not only highlights the possible role for *α,β*-unsaturated moiety of **2** in MurA inhibitory activities but also explains why **4** shows no activity on MurA. Although some experimental evidence is still missing, such as the identification of UNAG-**2** adduct, the biological data suggested that **2** still works well in fosfomycin-resistant strains (either in FosB-harboring or MurA (Cys-to-Asp) strains).

CONCLUSION

Four avenaciolides derivatives (**1**−**4**) were isolated from *N. fischeri*. **1**−**3** disrupt cell wall assembly through MurA inhibition. Importantly, **2** exhibits potent inhibitory activity against both wild-type and fosfomycin-resistant (Cys-to-Asp) MurA through either a covalent bond with the catalytic cysteine in MurA^{WT} or forming a "dead-end" adduct in MurA^{C119D} (Figure 6e).

With the alarming increase in multiple drug resistance, treating infections by combination therapies have become an unstoppable trend.[58−62] In clinical, the treatments for severe MRSA or other multiple-drug-resistant pathogens require not only the originally used antibiotics but also the combination of fosfomycin to facilitate efficacy.[59,62,63] Because **2** shows the potency toward fosfomycin-resistant model (*Ec*MurA^{C115D} overexpressed in *E. coli* BL21), **2** could also be used not only in combination therapies but also in treating fosfomycin-resistant pathogens.

To further develop **2** as a MRSA MurA inhibitor, we are investigating the structure−activity relationship of the compound to optimize the solubility and biological activity of avenaciolide derivatives. So far, we are attempting to co-crystallize MRSA MurA^{WT} and MurA^{C119D} in complex with **2** to apply structure-based drug design. Because MurA shares no homology with mammalian proteins, **2** may serve as a lead compound with little safety concerns.[7,64] Therefore, we believe **2** is a promising alternative for the post-antibiotic era.

EXPERIMENTAL SECTION

Antimicrobial Activity MIC Assays. *Acinetobacter baumannii*, *S. aureus*, *B. subtilis*, *E. coli* strains (defined in Table 1) were cultured on cation-adjusted Mueller-Hinton II (MH) agar or in MH broth (Becton Dickinson, cat. no. 212322). MIC assays were performed via broth microdilution in accordance with CLSI guidelines with the exceptions that the compound stocks were prepared at 50× final assay concentrations and that the MIC values were determined colorimetrically. The input inoculum for each strain was prepared by

DOI: 10.1021/ja510375f
J. Am. Chem. Soc. 2015, 137, 267−275

resuspending cells grown on agar plates in phosphate-buffered saline (PBS) to an OD 600 of 0.10. A volume of this suspension was added to the appropriate broth media at a final concentration of 5×10^5 colony-forming units (CFU)/mL. Then, 98 μL of the broth + cell solution for each strain was added to each well of a 96-well assay plate (Costar, cat. no. 3370). Solutions of avenociolide analogues were freshly prepared in 100% dimethyl sulfoxide (DMSO) prior to use. Compound stock solutions were then serially diluted in 2-fold steps in DMSO, resulting in final test concentrations of 0.004−256 μg mL^{-1} when diluted 1:50 in test broth (addition of 2 μL of compound stock to 98 μL of broth + cells). The initial inoculum for each strain was serially diluted in PBS and plated on appropriate agar media to ensure that the assay contained the approximate desired number of CFU. MIC assay plates were incubated overnight at 37 °C under aerobic conditions for all strains.

TEM. To investigate the possible mechanisms of action of the active compounds against bacteria, thin-layer TEM was performed. Exponential-phase bacteria were treated with compounds at 4× MIC for 1 h at 37 °C. Then, the cells were washed twice, resuspended in PBS, and fixed with 2.5% glutaraldehyde in 0.1 M cacodylate. The samples were then incubated at 4 °C for at least 1 h. After incubation, the cells were recovered by centrifugation at 10,000 *g* for 5 min and washed twice with PBS. The pellets were fixed with 1% osmium tetraoxide and incubated at room temperature for 1 h. The samples were dehydrated with graded ethanol solutions: 30% ethanol for 10 min, 50% ethanol for 10 min, 70% ethanol for 10 min, 90% ethanol for 10 min, and twice in 100% ethanol for 15 min. The samples were fixed in Epon 812 resin and allowed to polymerize for 3 days. Each sample was cut into thin slices of approximately 90 nm with a glass knife and stained with uranyl acetate and lead citrate on grids. The morphological and ultrastructural properties of the bacteria were observed and photographed using an FEI Technai G2 F20 S-Twin at 75 kV.

Characterization of the Inhibitory Activity of Avenaciolide Analogues Against MurA by a ^{31}P NMR Spectroscopy-Based Method. The avenaciolides **1**−**4** (10 μL, stock solution 10 mM in DMSO) or fosfomycin (10 μL, stock solution 10 mM in H_2O) were incubated with protein (3.68 μM of MRSA MurA^{WT} and 5.6 μM of MRSA MurA^{C119D}) in buffer containing 50 mM HEPES (pH 7.6), 0.125% BSA, 600 μM UNAG, and 800 μM PEP at 37 °C for 1 h. All reactions were initialized by adding PEP under the same conditions with 10% DMSO and D_2O. Then, ^{31}P NMR spectra were acquired at 303 K on a Bruker AVANCE 500 NMR spectrometer, operating at 11.7 T, observing ^{31}P at 202 MHz, equipped with a 5 mm direct detection probe with *z* gradient. The spectra were acquired by applying 30° excitation pulses with ^{1}H decoupling during acquisition with 32 *k* data points, a spectral resolution of 2.29 Hz, 128 scans averages, and a recycle time of 0.2 s. All NMR spectra were manually phased, baseline corrected, and referenced against the PEP ^{31}P NMR signal at δ −1.06.

The Reaction of Avenaciolide Analogues with Cysteine and Glutathione (GSH). Because the reactivity of the avenaciolide analogues and the sulfhydryl group of cysteine has not been previously studied, we proposed that the α,β-unsaturated carbonyl moiety would be attacked by the sulfhydryl group of Cys119 in MRSA MurA. To investigate the reactivity of compounds **1**−**3** and their covalent-adduct products toward thiols, we used L-cysteine and glutathione (GSH) as sulfhydryl nucleophile models to simulate the SH group of Cys119 in MRSA MurA. Compounds **1**−**3** (10 μL, stock solution 10 mM in DMSO) and 10 μL of GSH/cysteine (stock solution 10 mM in H_2O) were dissolved in 980 μL of sodium citrate buffer (50 mM pH 8.0), resulting in final concentrations of 100 μM. Aliquots (100 μL) of the reaction mixture were withdrawn at regular intervals (at 1, 5, and 10 min) and quenched with 1 μL of *ortho*-phosphoric acid (85%). The samples were analyzed by LC-ESI-MS and LC-ESI-MS/MS.

Peptide Mapping, Mass Spectrometry, and Sequencing of Avenaciolide-Labeled Peptides in Inactivated MurA. To examine covalent adduct formation, 100 μL of incubation mixture containing 42 μM MurA in 50 mM Tris pH 8.0, 5 mM DTT, and 1 mM avenaciolides was incubated at 25 °C for 1 h. The samples were desalted, and free compound was removed using MicroSpin G-50 columns (Amersham Pharmacia Biotech, Parsippany, NJ). Trypsin or chymotrypsin was then added to these solutions to maintain a substrate-to-enzyme ratio of 25:1 (w/w), and the mixture was incubated at 37 °C for 16−20 h. The resultant peptide mixtures were frozen at −20 °C until separation by reverse-phase UPLC-ESI-MS. Tryptic or chymotryptic peptides were detected using reverse-phase UPLC-ESI-MS on a LTQ Orbitrap XL ETD mass spectrometer (Thermo Fisher Scientific, San Jose, CA) equipped with a Waters ACQUITY UPLC using an ACQUITY UPLC CSH130 C18 column (1.0 × 150 mm, 1.7 mm, Waters, Milford, MA). Briefly, the gradient was 5% buffer B (95% buffer A) from 0 to 1 min, 40% buffer B (60% buffer A) at 40 min, 98% buffer B (2% buffer A) at 41 min, and 98% buffer B (2% buffer A) at 50 min with a flow rate of 50 μL min^{-1}. Buffer A was 0.1% formic acid/H_2O and buffer B was 0.1% formic acid/acetonitrile. The survey full-scan MS conditions were as follows: mass range m/z 320−2000 and resolution 30,000 at m/z 400. The three most intense ions were sequentially isolated for HCD (Resolution 7500). The electrospray voltage was maintained at 4.0 kV, and the capillary temperature was set at 275 °C. The data were processed using MaxQuant[65] version 1.3.0.5, and the peptides were identified by searching the MS/MS spectra against the MRSA MurA protein (user defined) using the Andromeda search engine.[66] Cysteine alkylation was used as a fixed modification, and the modification m/z values were 266, 298, and 284, respectively, for compounds **1**, **2**, and **3**. For identification, the false discovery rate was set to 0.01 for peptides, proteins, and sites, and the minimum peptide length allowed was six amino acids.

MurA Assay. In a standardized assay, MurA enzymes (MRSA and *E. coli*) were preincubated with the substrate UNAG and an inhibitor for 10 min at 37 °C. To determine the influence of UNAG on the binding process, experiments were performed in the absence of UNAG during preincubation. The reaction was initiated by the addition of the second substrate PEP, resulting in a total volume of 100 μL with the following concentrations: *E. coli* MurA or MRSA MurA 25 nM, UNAG 310 μM, PEP 620 μM, 50 mM HEPES pH 7.6, DMSO 1% (v/v). The reaction was stopped after 60 min at 37 °C by adding 100 μL of Lanzetta reagent[34] containing malachite green solution (0.045% (w/v)) and ammonium heptamolybdate (8.4% (w/v) in 8 N HCl) at a ratio of 3:1 and with 0.03% (w/v) Tergitol NP-40 as dye-stabilizing detergent. After 10 min, the absorbance at 620 nm was measured using a FlexStation 3 Microplate Reader (Molecular Devices). Finally, dose−response curves were generated by measuring the enzyme activity of five replicates at least eight different compound concentrations. The assays were performed as described above. The resulting data were plotted using GraphPad Prism version 6.0 (GraphPad Software, San Diego, California), and IC_{50} values indicating the concentration of the compound with a residual activity of 50% were determined from a four-parameter fit model.

3D-Model Structure of *S. aureus* (strain ATCC33592) MurA. The 3D-homology model of *S. aureus* MurA was generated using Discovery Studio (Accelrys Software Inc.) based on the structures of the MurAs from *E. cloacae* (PDB code 1EJC), *E. cloacae* (3KQJ), *E. coli* (1UAE), *E. coli* K12 (3SWD), *H. influenzae* Rd KW20 (3SWE), and *S. pneumoniae* D39 (3ZH3) as templates. *S. aureus* MurA shares ∼40% sequence identity with these templates. The resulting model of *S. aureus* MurA was optimized by energy minimization using the Discovery Studio program, and the stereochemical quality of the model was further verified using the 3D-profile and PROCHECK programs.[67,68]

Molecular Simulation. Based on the binding mode of fosfomycin to *E. coli* MurA,[52] the model of compound **2** was manually docked into the active site of *S. aureus* MurA using the Coot program[69] to generate an initial binding pose from which the catalytic cysteine Cys119 forms a covalent linkage to the compound. The molecular simulation was performed using Discovery Studio, and the CHARM force field was applied to the molecule. The model of the *S. aureus* MurA-**2** complex was simulated using the "Standard Dynamics Cascade" protocol, which consists of two rounds of minimization, heating, equilibration, and production for 1 ns. During the simulation, the distance for the

DOI: 10.1021/ja510375f
J. Am. Chem. Soc. 2015, 137, 267−275

covalent linkage between *S. aureus* and MurA was fixed, and the heating temperature was set at 50−300 K. The final model was also verified using 3D-profile and PROCHECK. The structure figures were generated using the PyMOL program (Schrödinger, New York, NY, USA).

■ ASSOCIATED CONTENT

Supporting Information

Supplemental results, microbiological procedures, characterizations and interpretation of avenaciolides **1**−**4**, MS/MS spectra. This material is available free of charge via the Internet at http://pubs.acs.org.

■ AUTHOR INFORMATION

Corresponding Author

shwu@gate.sinica.edu.tw

Notes

The authors declare no competing financial interest.

■ ACKNOWLEDGMENTS

We thank the Cryo-EM Common Facility of the Scientific Instrument Center, Academic Sinica, for transmission electron microscopy services and Dr. Ting-Jen Cheng (Genomics Research Center, Academia Sinica, Taipei, Taiwan) for assistance with performing the MIC experiments. We are grateful to Dr. Feng-Ling Yang for critically reading the manuscript. This work was supported by the grants (NSC 100-2113-M-001-022-MY3 and MOST 103-2113-M-001-029-MY3)

■ REFERENCES

(1) Levy, S. B.; Marshall, B. *Nat. Med.* **2004**, *10*, S122.
(2) Malachowa, N.; DeLeo, F. *Cell. Mol. Life Sci.* **2010**, *67*, 3057.
(3) Schito, G. C. *Clin. Microbiol. Infect.* **2006**, *12*, 3.
(4) DeLeo, F. R.; Chambers, H. F. *J. Clin. Invest.* **2009**, *119*, 2464.
(5) Morell, E. A.; Balkin, D. M. *Yale J. Biol. Med.* **2010**, *83*, 223.
(6) Payne, D. J. *Science* **2008**, *321*, 1644.
(7) Silver, L. L. *Biochem. Pharmacol.* **2006**, *71*, 996.
(8) Bugg, T. D. H.; Walsh, C. T. *Nat. Prod. Rep.* **1992**, *9*, 199.
(9) Brown, E. D.; Vivas, E. I.; Walsh, C. T.; Kolter, R. *J. Bacteriol.* **1995**, *177*, 4194.
(10) Du, W.; Brown, J. R.; Sylvester, D. R.; Huang, J.; Chalker, A. F.; So, C. Y.; Holmes, D. J.; Payne, D. J.; Wallis, N. G. *J. Bacteriol.* **2000**, *182*, 4146.
(11) Blake, K. L.; O'Neill, A. J.; Mengin-Lecreulx, D.; Henderson, P. J. F.; Bostock, J. M.; Dunsmore, C. J.; Simmons, K. J.; Fishwick, C. W. G.; Leeds, J. A.; Chopra, I. *Mol. Microbiol.* **2009**, *72*, 335.
(12) De Smet, K. A. L.; Kempsell, K. E.; Gallagher, A.; Duncan, K.; Young, D. B. *Microbiology* **1999**, *145*, 3177.
(13) McCoy, A. J.; Sandlin, R. C.; Maurelli, A. T. *J. Bacteriol.* **2003**, *185*, 1218.
(14) Jiang, S.; Gilpin, M. E.; Attia, M.; Ting, Y.-L.; Berti, P. J. *Biochemistry* **2011**, *50*, 2205.
(15) Nikolaidis, I.; Favini-Stabile, S.; Dessen, A. *Protein Sci.* **2014**, *23*, 243.
(16) Arca, P.; Rico, M.; Braña, A. F.; Villar, C. J.; Hardisson, C.; Suárez, J. E. *Antimicrob. Agents Chemother.* **1988**, *32*, 1552.
(17) Horii, T.; Kimura, T.; Sato, K.; Shibayama, K.; Ohta, M. *Antimicrob. Agents Chemother.* **1999**, *43*, 789.
(18) Venkateswaran, P. S.; Wu, H. C. *J. Bacteriol.* **1972**, *110*, 935.
(19) Qu, T-t.; Shi, K.-r.; Ji, J.-s.; Yang, Q.; Du, X.-x.; Wei, Z.-q.; Yu, Y.-s. *Int. J. Antimicrob. Agents* **2013**, *43*, 361.
(20) Nicolle, L. E. *Am. J. Med.* **2002**, *113*, 35.
(21) Hendlin, D.; Stapley, E. O.; Jackson, M.; Wallick, H.; Miller, A. K.; Wolf, F. J.; Miller, T. W.; Chaiet, L.; Kahan, F. M.; Foltz, E. L.; Woodruff, H. B.; Mata, J. M.; Hernandez, S.; Mochales, S. *Science* **1969**, *166*, 122.
(22) Marquardt, J. L.; Brown, E. D.; Lane, W. S.; Haley, T. M.; Ichikawa, Y.; Wong, C.-H.; Walsh, C. T. *Biochemistry* **1994**, *33*, 10646.
(23) Wanke, C.; Amrhein, N. *Eur. J. Biochem.* **1993**, *218*, 861.
(24) Kahan, F. M.; Kahan, J. S.; Cassidy, P. J.; Kropp, H. *Ann. N.Y. Acad. Sci.* **1974**, *235*, 364.
(25) Etienne, J.; Gerbaud, G.; Courvalin, P.; Fleurette, J. *FEMS Microbiol. Lett.* **1989**, *61*, 133.
(26) Roberts, A. A.; Sharma, S. V.; Strankman, A. W.; Duran, S. R.; Rawat, M.; Hamilton, C. J. *Biochem. J.* **2013**, *451*, 69.
(27) Etienne, J.; Gerbaud, G.; Fleurette, J.; Courvalin, P. *FEMS Microbiol. Lett.* **1991**, *84*, 119.
(28) Cao, M.; Bernat, B. A.; Wang, Z.; Armstrong, R. N.; Helmann, J. D. *J. Bacteriol.* **2001**, *183*, 2380.
(29) Bauer, A.; Bronstrup, M. *Nat. Prod. Rep.* **2014**, *31*, 35.
(30) Schmitt, E. K.; Moore, C. M.; Krastel, P.; Petersen, F. *Curr. Opin. Chem. Biol.* **2011**, *15*, 497.
(31) Rodicio, M.-R.; Manzanal, M.-B.; Hardisson, C. *Arch. Microbiol.* **1978**, *118*, 219.
(32) Bachelier, A.; Mayer, R.; Klein, C. D. *Bioorg. Med. Chem. Lett.* **2006**, *16*, 5605.
(33) Mendgen, T.; Scholz, T.; Klein, C. D. *Bioorg. Med. Chem. Lett.* **2010**, *20*, 5757.
(34) Lanzetta, P. A.; Alvarez, L. J.; Reinach, P. S.; Candia, O. A. *Anal. Biochem.* **1979**, *100*, 95.
(35) Kadner, R. J.; Winkler, H. H. *J. Bacteriol.* **1973**, *113*, 895.
(36) Castañeda-García, A.; Rodríguez-Rojas, A.; Guelfo, J. R.; Blázquez, J. *J. Bacteriol.* **2009**, *191*, 6968.
(37) Santoro, A.; Cappello, A. R.; Madeo, M.; Martello, E.; Iacopetta, D.; Dolce, V. *Biochim. Biophys. Acta* **2011**, *1810*, 1323.
(38) Potashman, M. H.; Duggan, M. E. *J. Med. Chem.* **2009**, *52*, 1231.
(39) Leproult, E.; Barluenga, S.; Moras, D.; Wurtz, J.-M.; Winssinger, N. *J. Med. Chem.* **2011**, *54*, 1347.
(40) Liu, Q.; Sabnis, Y.; Zhao, Z.; Zhang, T.; Buhrlage, S. J.; Jones, L. H.; Gray, N. S. *Chem. Biol.* **2013**, *20*, 146.
(41) Singh, J.; Petter, R. C.; Baillie, T. A.; Whitty, A. *Nat. Rev. Drug. Discovery* **2011**, *10*, 307.
(42) Smith, A. J. T.; Zhang, X.; Leach, A. G.; Houk, K. N. *J. Med. Chem.* **2008**, *52*, 225.
(43) Wissner, A.; Overbeek, E.; Reich, M. F.; Floyd, M. B.; Johnson, B. D.; Mamuya, N.; Rosfjord, E. C.; Discafani, C.; Davis, R.; Shi, X.; Rabindran, S. K.; Gruber, B. C.; Ye, F.; Hallett, W. A.; Nilakantan, R.; Shen, R.; Wang, Y.-F.; Greenberger, L. M.; Tsou, H.-R. *J. Med. Chem.* **2002**, *46*, 49.
(44) Kim, D. H.; Lees, W. J.; Kempsell, K. E.; Lane, W. S.; Duncan, K.; Walsh, C. T. *Biochemistry* **1996**, *35*, 4923.
(45) Brown, E. D.; Marquardt, J. L.; Lee, J. P.; Walsh, C. T.; Anderson, K. S. *Biochemistry* **1994**, *33*, 10638.
(46) Jackson, S. G.; Zhang, F.; Chindemi, P.; Junop, M. S.; Berti, P. J. *Biochemistry* **2009**, *48*, 11715.
(47) Clark, M. E.; Berti, P. J. *Biochemistry* **2007**, *46*, 1933.
(48) Engel, H.; Gutiérrez-Fernández, J.; Flückiger, C.; Martínez-Ripoll, M.; Mühlemann, K.; Hermoso, J. A.; Hilty, M.; Hathaway, L. J. *Antimicrob. Agents Chemother.* **2013**, *57*, 2801.
(49) Eschenburg, S.; Schönbrunn, E. *Proteins: Struct., Funct. Bioinf.* **2000**, *40*, 290.
(50) Han, H.; Yang, Y.; Olesen, S. H.; Becker, A.; Betzi, S.; Schönbrunn, E. *Biochemistry* **2010**, *49*, 4276.
(51) Yoon, H.-J.; Lee, S. J.; Mikami, B.; Park, H.-J.; Yoo, J.; Suh, S. W. *Proteins: Struct., Funct. Bioinf.* **2008**, *71*, 1032.
(52) Skarzynski, T.; Mistry, A.; Wonacott, A.; Hutchinson, S. E.; Kelly, V. A.; Duncan, K. *Structure (London)* **1996**, *4*, 1465.
(53) Eschenburg, S.; Priestman, M.; Schönbrunn, E. *J. Biol. Chem.* **2005**, *280*, 3757.
(54) Schönbrunn, E.; Eschenburg, S.; Krekel, F.; Luger, K.; Amrhein, N. *Biochemistry* **2000**, *39*, 2164.
(55) Samland, A. K.; Etezady-Esfarjani, T.; Amrhein, N.; Macheroux, P. *Biochemistry* **2001**, *40*, 1550.
(56) Zhu, J.-Y.; Yang, Y.; Han, H.; Betzi, S.; Olesen, S. H.; Marsilio, F.; Schönbrunn, E. *J. Biol. Chem.* **2012**, *287*, 12657.

DOI: 10.1021/ja510375f
J. Am. Chem. Soc. 2015, 137, 267−275

(57) Steinbach, A.; Scheidig, A. J.; Klein, C. D. *J. Med. Chem.* **2008**, *51*, 5143.
(58) Fleming, E.; Heil, E. L.; Hynicka, L. M. *Ann. Pharmacother.* **2014**, *48*, 123.
(59) Burke, S. L.; Rose, W. E. *Expert Opin. Pharmacother.* **2014**, 1.
(60) Wilke, M.; Grube, R. *Infect. Drug Resist.* **2013**, *7*, 1.
(61) Corvec, S.; Furustrand Tafin, U.; Betrisey, B.; Borens, O.; Trampuz, A. *Antimicrob. Agents Chemother.* **2013**, *57*, 1421.
(62) Lee, W.-S.; Chen, Y.-C.; Chen, H.-P.; Chen, T.-H.; Cheng, C.-Y. *J. Microbiol. Immunol. Infect.* **2013**, 1684.
(63) Oliva, A.; Tafin, U. F.; Maiolo, E. M.; Jeddari, S.; Bétrisey, B.; Trampuz, A. *Antimicrob. Agents Chemother.* **2013**, *57*, 1421.
(64) Hao, H.; Cheng, G.; Dai, M.; Wu, Q.; Yuan, Z. *Mol. BioSyst.* **2012**, *8*, 2828.
(65) Cox, J.; Mann, M. *Nat. Biotechnol.* **2008**, *26*, 1367.
(66) Cox, J. r.; Neuhauser, N.; Michalski, A.; Scheltema, R. A.; Olsen, J. V.; Mann, M. *J. Proteome Res.* **2011**, *10*, 1794.
(67) Emsley, P.; Cowtan, K. *Acta Crystallogr., Sect. D: Biol. Crystallogr.* **2004**, *60*, 2126.
(68) Luthy, R.; Bowie, J. U.; Eisenberg, D. *Nature* **1992**, *356*, 83.
(69) Laskowski, R. A.; Moss, D. S.; Thornton, J. M. *J. Mol. Biol.* **1993**, *231*, 1049.

DOI: 10.1021/ja510375f
J. Am. Chem. Soc. 2015, 137, 267−275